

EFFECTS OF CONVECTION ON THE MEAN SOLAR STRUCTURE

JØRGEN CHRISTENSEN-DALSGAARD
*Teoretisk Astrofysik Center, Danmarks Grundforskningsfond,
and
Institut for Fysik og Astronomi, Aarhus Universitet,
DK-8000 Aarhus C, Denmark*

Abstract. The overall framework for the study of solar convection and oscillations is the spherically symmetric component of solar structure. I discuss those properties of the solar interior which depend on convection and other possible hydrodynamical motion and the increasingly detailed information about the structure which is provided by helioseismic data. The most basic dependence of solar models on convection is the calibration to fix the solar radius. The dominant causes for differences in oscillation frequencies between the Sun and solar models seem to be located near the top of the convection zone. However, there is also evidence for possible weak mixing below the convection zone and perhaps in the solar core. The former, at least, might be induced by penetration of convective motion into the stable layers below.

Key words: solar structure, convection, helioseismology

1. Introduction

The outer solar convection zone extends over 29 % of the solar radius and contains about 2 % of the mass of the Sun (*e.g.* Christensen-Dalsgaard, Gough & Thompson 1991; Kosovichev & Fedorova 1991). Within most of this region, energy transport is dominated by convection, leading to a temperature gradient which only deviates slightly from being adiabatic. In particular, the structure of the convection zone is essentially independent of the local value of the opacity. Furthermore, matter is mixed on a time scale of months and hence the composition may be assumed to be uniform.

In earlier phases of solar evolution, the convection zone has extended considerably more deeply: thus it is normally assumed that the Sun was fully convective before arriving on the main sequence, justifying the assumption that the early Sun was chemically homogeneous.

Motion induced by convection is likely to extend beyond the boundaries of the convection zone. This can be observed in the solar atmosphere and has a significant effect on the atmospheric structure. Penetration beneath the lower boundary of the convection zone can only be inferred indirectly, but is potentially far more important for overall solar structure and evolution. It may affect the temperature stratification in the upper parts of the radiative interior and cause mixing and transport of angular momentum, either through direct motion in the form of penetrating convective plumes or through convectively induced gravity waves (*e.g.* Schatzman, these proceedings; Zahn, these proceedings). Clear evidence for such mixing is provided by the solar surface abundances of lithium and beryllium which are considerably reduced (by factors of about 140 and 2, respectively; Anders & Grevesse 1989), relative to the initial composition of the solar system; this indicates that matter has been mixed to a temperature considerably higher than the maximum temperature at the base of the convectively unstable region during the main-sequence life of the Sun.

Here I am concerned with the effects of convection on the spherically symmetric stellar structure and evolution, and how these effects can be investigated through observations of solar oscillations. Many of these issues will be addressed in more detail in later papers in the present volume; however, I hope to provide a general framework, as well as a basic impression of the data now available for testing the solar models.

Gough & Weiss (1976) pointed out that the properties of the convection zone is essentially controlled by the thin, substantially superadiabatic region at its top. The integral of the superadiabatic gradient over this region determines the adiabat of the nearly adiabatic part of the convection zone and hence its overall structure. Provided the treatment of the superadiabatic region is adjusted, *e.g.* by varying suitable parameters, such as to yield the same adiabat, the overall structure is insensitive to the details of that treatment. Here I consider two simple parametrized treatments of convection. One is the mixing-length theory of Böhm-Vitense (1958; in the following MLT), with a mixing length proportional to the pressure scale height. The second is the formulation by Canuto & Mazzitelli (1991; CM), with a characteristic scale related to the distance to the top of the convection zone. A potentially more realistic description of the superadiabatic region can in principle be based on appropriate averages of numerical solutions of the time-dependent hydrodynamical equations of convection. I shall consider results of simulations carried out by Nordlund, Stein and

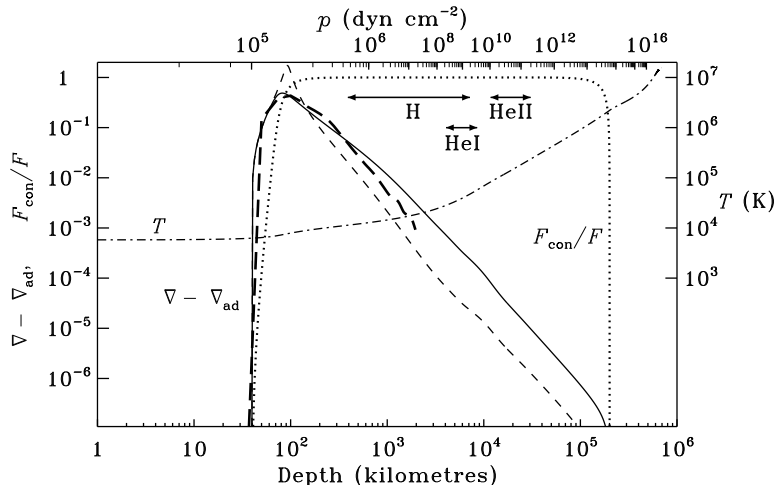


Figure 1. Properties of the solar convection zone. The lower abscissa is depth below the point in the atmosphere where the temperature equals the effective temperature, whereas the upper abscissa is pressure p . Most of the results are based on Model S of Christensen-Dalsgaard *et al.* (1996), which used the Böhm-Vitense (1958) mixing-length theory. The dot-dashed curve, using the right-hand ordinate scale, shows temperature T . The remaining quantities refer to the left-hand ordinate scale. The solid curve shows the superadiabatic temperature gradient $\nabla - \nabla_{\text{ad}}$, where $\nabla = d \ln T / d \ln p$ and $\nabla_{\text{ad}} = (\partial \ln T / \partial \ln p)_s$, the derivative being at constant specific entropy s . The dotted curve shows the convective flux F_{con} , in units of the total flux F . The horizontal arrows indicate the locations of the ionization zone of hydrogen and the first and second ionization zones of helium, extending between the points of 10 and 90 % ionization. In addition, the short-dashed curve shows $\nabla - \nabla_{\text{ad}}$ for a model using the Canuto & Mazzitelli (1991) treatment of convection, and the heavy long-dashed curve shows $\nabla - \nabla_{\text{ad}}$ in the average model resulting from hydrodynamical simulations (Stein & Nordlund 1989; Nordlund, these proceedings). (Adapted from Gough & Weiss 1976).

Trampedach (*e.g.* Stein & Nordlund 1989; Nordlund, these proceedings; Trampedach *et al.*, these proceedings). Unlike the simple formulations, this does not contain explicitly adjustable parameters; hence it provides a prediction of the adiabat.

An overview of the structure of the solar convection zone is provided by Fig. 1, in a form originally introduced by Gough & Weiss (1976). This is based mostly on Model S of Christensen-Dalsgaard *et al.* (1996); the model was computed with the OPAL opacity (Iglesias, Rogers & Wilson 1992) and equation of state (Rogers, Swenson & Iglesias 1996) and included settling and diffusion of helium and heavy elements, using coefficients from Michaud & Proffitt (1993). Convection was treated using the MLT. In addition, the figure shows superadiabatic gradients obtained with the calibrated CM formulation and the hydrodynamical simulations. It is evident that in all

cases the region of substantially superadiabatic convection is restricted to the outer few hundred kilometres of the convection zone.

2. The structure of the solar convection zone

As illustrated by Fig. 1 the region of significant superadiabaticity is extremely thin, compared with the extent of the solar convection zone. Thus the detailed structure of this region matters little insofar as the overall structure of the star is concerned. However, it provides the transition between the stellar atmosphere and the almost adiabatic bulk of the convection zone. The structure of the atmosphere can be found observationally, in terms of semi-empirical atmospheric models. Thus the integral over the superadiabatic gradient, which determines the change in specific entropy between the atmosphere and the interior of the convection zone, essentially fixes the adiabat of the adiabatic part of the convection zone. This, together with the equation of state and composition, largely determines the structure of the convection zone.

The structure of the upper parts of the convection zone is also affected by the dynamical effects of convection, generally represented as a *turbulent pressure* (see Rosenthal, these proceedings; Antia & Basu, these proceedings). These effects are often neglected in calculations of stellar models, however.

2.1. PROPERTIES OF THE CONVECTION ZONE

To illustrate the properties of the convection zone it is instructive to consider a highly simplified model. I assume the equation of state for a fully ionized perfect gas; then the adiabatic relation between pressure p and density ρ can be written as

$$p = K\rho^\gamma, \quad (1)$$

where γ and K may be assumed to be constant. Neglecting also the mass contained in the convection zone the equation of hydrostatic support is

$$\frac{dp}{dr} = -\frac{GM\rho}{r^2}, \quad (2)$$

where r is distance to the centre of the star, M is the mass of the star and G is the gravitational constant. From equations (1) and (2) one obtains

$$GM \left(\frac{1}{r} - \frac{1}{R_*} \right) = K^{1/\gamma} \frac{\gamma}{\gamma - 1} \left[p^{1-1/\gamma} - p_*^{1-1/\gamma} \right], \quad (3)$$

where p_* is the pressure at a point near the top of the convection zone and $R_* \simeq R$ is the radius at this point, R being the surface radius of the star.

Conditions at the base of the convection zone are determined by the transition to convective stability, where matching to the radiative interior fixes the radius r_{cz} and pressure p_{cz} at the convection-zone base. The condition of marginal convective instability is

$$\frac{3}{16\pi a \tilde{c} G} \frac{\kappa p}{T^4} \frac{L}{M} = \nabla_{\text{ad}} , \quad (4)$$

where a is the radiation density constant, \tilde{c} is the speed of light, T is temperature, L is luminosity, κ is opacity, and we neglected again the mass in the convection zone; also $\nabla_{\text{ad}} \simeq 2/5$. This condition, together with equation (1), the equation of state and the dependence of κ on p and T , determines the relation between K and p_{cz} . It is most simply analyzed by considering the response of the model to a change δK in K , keeping the other parameters of the model, including mass and composition, fixed. As confirmed by numerical computations, changes in the convective envelope and outer part of the radiative interior have little effect on the energy-generating core; thus L is largely unchanged and so therefore, according to equation (4), is $\kappa p/T^4$. Using the ideal gas law and equation (1) we therefore obtain

$$0 \simeq \delta \ln \left(\frac{\kappa p}{T^4} \right) = \frac{\kappa_T - 4}{\gamma} \delta \ln K + \frac{1}{\gamma} [(\kappa_T - 4)(\gamma - 1) + \gamma(\kappa_p + 1)] \delta \ln p_{\text{cz}} , \quad (5)$$

where $\kappa_p = (\partial \ln \kappa / \partial \ln p)_T$ and $\kappa_T = (\partial \ln \kappa / \partial \ln T)_p$; thus

$$\delta \ln p_{\text{cz}} \simeq - \frac{4 - \kappa_T}{(4 - \kappa_T)(\gamma - 1) - \gamma(\kappa_p + 1)} \delta \ln K . \quad (6)$$

At the base of the solar convection zone, $\kappa_p \simeq 0.58$ and $\kappa_T \simeq -3.61$. Thus, using $\gamma = 5/3$, we find that $\delta \ln p_{\text{cz}} \simeq -3.1 \delta \ln K$.

We may now use equation (3) to find the resulting change in R . Assuming that $p_{\text{cz}} \gg p_*$ and $R_* \simeq R$, we have that

$$GM \left(\frac{1}{r_{\text{cz}}} - \frac{1}{R} \right) \simeq K^{1/\gamma} \frac{\gamma}{\gamma - 1} p_{\text{cz}}^{1-1/\gamma} . \quad (7)$$

The change in p_{cz} evidently causes a change in r_{cz} ; assuming that the hydrostatic structure of the interior, defined by $p(r)$, changes little up to the base of the convection zone,

$$\delta r_{\text{cz}} \simeq -H_p \delta \ln p_{\text{cz}} , \quad (8)$$

where H_p is the pressure scale height evaluated at the base of the convection zone. From equation (7) it therefore follows that

$$\delta R = - \left(\frac{R}{r_{\text{cz}}} \right)^2 H_p \delta \ln p_{\text{cz}} + \frac{R}{r_{\text{cz}}} d_{\text{cz}} \delta \ln \left(K^{1/\gamma} p_{\text{cz}}^{1-1/\gamma} \right) , \quad (9)$$

where $d_{cz} = R - r_{cz}$ is the depth of the convection zone. Using again solar values, *i.e.*, $r_{cz} \simeq 0.71R$, $H_p \simeq 0.081R$, and the relation obtained above between $\delta \ln p_{cz}$ and $\delta \ln K$, we find, separating the contributions from the two terms in equation (9)

$$\frac{\delta R}{R} \simeq 0.50 \delta \ln K - 0.26 \delta \ln K = 0.24 \delta \ln K , \quad (10)$$

and hence

$$\frac{\delta d_{cz}}{R} \simeq -0.02 \delta \ln K . \quad (11)$$

It is remarkable, and perhaps surprising, that in the solar case the depth of the convection zone appears to be virtually insensitive to changes in the adiabat of the convection zone, the change in surface radius resulting from the change in the radius at the base of the convection zone. As discussed below, this is confirmed by numerical results for solar models. Note also that H_p is approximately proportional to depth; thus it is likely that the relative magnitude of the two terms in equation (9), and hence the sign of the relation in equation (10) will be roughly the same for other stars, at least as long as the opacity derivatives do not change substantially.

2.2. CALIBRATION OF THE SURFACE RADIUS

The dependence of R on K is used to calibrate solar models to have the observed radius, by adjusting K . This might most simply be achieved by assuming a discontinuity in ρ and T at the top of the convection zone such that K attains the correct value (*e.g.* Schwarzschild 1958). However, more commonly a simplified physical description of convection is used, generally containing a parameter which can be adjusted to ensure the correct radius; this might allow a safer extrapolation from the solar case, where such calibration can be made, to models of other stars where this is rarely possible.

The main features of this calibration can be illustrated by noting that in the deeper part of the convection zone where matter is essentially fully ionized, K is related to the specific entropy by

$$s \simeq \frac{3}{5} c_p \ln K , \quad (12)$$

choosing the zero-point of entropy appropriately, where c_p is the specific heat at constant pressure, and γ was set to $5/3$. The value s_{ad} of s in adiabatic part of the convection zone is related to the photospheric value s_{ph} by $s_{ad} = s_{ph} + \Delta s$, where

$$\Delta s = \int_{\ln p_{ph}}^{\ln p^*} c_p (\nabla - \nabla_{ad}) d \ln p ; \quad (13)$$

here p^* is a suitable point in the convection zone, such that $\nabla - \nabla_{\text{ad}} \ll 1$. Assuming that the atmospheric structure is approximately unchanged, the change in K is obtained from the change in Δs as

$$\delta \ln K \simeq \frac{5}{3} \frac{\delta(\Delta s)}{c_p} . \quad (14)$$

For a given energy flux, $\nabla - \nabla_{\text{ad}}$ is determined by the efficacy of convection in the superadiabatic region: if convective transport becomes more efficient, the superadiabatic gradient is reduced, and so therefore is Δs and hence K , which according to equation (10) leads to a smaller radius of the model.

Several formulations of convection, including the commonly used mixing-length theory, determine the convective efficacy in terms of a characteristic scale ℓ , such as the size or mean free path of a convective element. This is often parametrized as a multiple α_c of a typical length scale in the model, such as the local pressure scale height or the distance to the boundary of the convection zone. In the limit of efficient convection, relevant to the larger part of the solar convection zone, the convective flux then satisfies $F_{\text{con}} \propto (\nabla - \nabla_{\text{ad}})^{3/2} \alpha_c^2$. It follows that if the luminosity, and hence approximately the convective flux, is kept fixed, $\nabla - \nabla_{\text{ad}} \propto \alpha_c^{-4/3}$. According to equations (13) and (14) we therefore have that

$$\delta \ln K \simeq -2 \frac{\Delta s}{c_p} \delta \ln \alpha_c \simeq -\delta \ln \alpha_c , \quad (15)$$

where the last equality used solar values for Δs ; hence, from equation (10),

$$\delta \ln R \simeq -0.24 \delta \ln \alpha_c . \quad (16)$$

2.3. RESULTS FOR STELLAR MODELS

To illustrate the behaviour of convective envelopes discussed in sections 2.1 and 2.2, I have calculated three static models, based on the composition profile of Model S (Christensen-Dalsgaard *et al.* 1996). Some properties of the models are summarized in Table 1. Models 1 and 2 have been calibrated to solar radius and luminosity by adjusting the convective efficacy and scaling the hydrogen abundance, as a function of mass, by a suitable factor (*e.g.* Christensen-Dalsgaard & Thompson 1991). In all cases, the envelope hydrogen abundance by mass is $X_e \simeq 0.737$. Model 1 used a version of the Canuto & Mazzitelli (1991) convection formulation, with mixing-length ℓ proportional to the distance to the convection-zone boundary, but including a parameter which allows calibration to the precise solar radius. Model 2 used the Böhm-Vitense mixing-length treatment, with a mixing

length $\ell = \alpha_c H_p$ proportional to the pressure scale height. Model 3 is also based on the Böhm-Vitense formulation, but choosing a different mixing length; the composition is the same as for Model 2. For these models turbulent pressure was ignored. In addition, the table lists an envelope model (Model 4) obtained by matching to a hydrodynamical simulation, in the manner of Trampedach *et al.* (these proceedings); convection was treated using MLT, with α_c and a factor in the treatment of turbulent pressure adjusted to obtain a continuous match of pressure and density in the deepest part of the simulation. Thus the adiabat of the deep convection zone is fixed by the properties of the simulation. For this model the hydrogen abundance is $X_e \simeq 0.703$.

TABLE 1. Properties of static solar models treating convection with the Canuto & Mazzitelli formulation (CM) or the Böhm-Vitense mixing-length formulation (MLT), as well as an envelope matched continuously to results of hydrodynamical simulation (SIM). The radius R and d_{cz} of the convection zone are given in units of the solar radius $R_\odot = 6.9599 \times 10^{10}$ cm. For the remaining notation, see text.

Model		α_c	R/R_\odot	d_{cz}/R_\odot	Δs (cgs)	K (cgs)	p_{cz} dyn cm ⁻²
1	CM	–	1.0000	0.2886	1.881×10^8	9.12×10^{14}	5.76×10^{13}
2	MLT	1.9894	1.0000	0.2884	1.881×10^8	9.12×10^{14}	5.74×10^{13}
3	MLT	1.7894	1.0226	0.2883	2.069×10^8	9.87×10^{14}	4.46×10^{13}
4	SIM	–	1.0000	0.3037	1.953×10^8	7.49×10^{14}	9.19×10^{13}

Figure 2 shows the superadiabatic gradient and the integrated entropy change, calculated from equation (13). It is evident that the CM formulation leads to a much higher and sharper peak in $\nabla - \nabla_{\text{ad}}$, with a corresponding strongly confined change in Δs . However, with the calibration to solar radius, the value of the entropy in the adiabatic part of the convection zone, and hence the properties of the interior of the model, are essentially the same in Models 1 and 2, as shown in more detail by the results presented in Table 1. On the other hand, the decrease in α_c in Model 3, relative to Model 2, causes an increase in $\nabla - \nabla_{\text{ad}}$, a corresponding increase in Δs and hence an increase in the radius of the model. The magnitude of the relative change in R , 2.3 %, is quite close to what is predicted by the simple approximation (16). Also, it should be noticed that the depth d_{cz} of the convection zone has changed little, in accordance with equation (11).

The results for the hydrodynamical simulation, matched to an envelope model, cannot be interpreted as simply in terms of the results of sections 2.2 and 2.3. Equation (7) still holds; however, since for the envelope model R is fixed, the relation defines the change in the depth of the convection

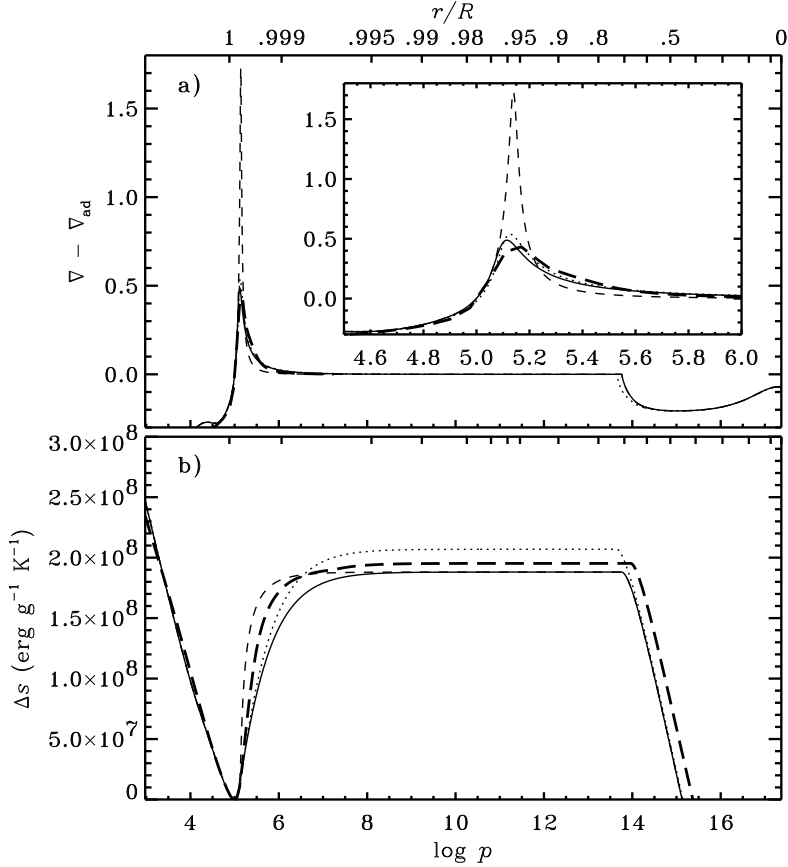


Figure 2. Superadiabatic gradient (a) and entropy difference Δs (b) in the four models listed in Table 1, using the following line styles: Model 1 (calibrated CM formulation) short-dashed line; Model 2 (calibrated MLT formulation) solid line; Model 3 (uncalibrated MLT formulation) dotted line; Model 4 (hydrodynamical simulation matched to MLT envelope) heavy long-dashed line. The lower abscissa is logarithmic (to base 10) of pressure, whereas the upper abscissa shows the corresponding fractional radius in Model 2. The insert in panel (a) shows details of the superadiabatic peak. In panel (b) the zero-point of Δs has been chosen at the top of the convection zone.

zone, as shown in Table 1. In this case one cannot assume that the interior is unaffected by the change in K , as was the case for complete models, and hence equation (8) is no longer valid. Also, because of the difference in composition between Models 2 and 4, say, there is no longer a simple connection between the changes in Δs and K . These questions deserve more careful study than can be attempted here, not least in connection with the calibration, described by Trampedach *et al.* (these proceedings), of the mixing length on the basis of convection simulations. It should be noticed also that the matched envelope predicts a convection zone extending

somewhat more deeply than in the calibrated models, as a result of the different value of K . Nevertheless, given the fact that no attempt was made in the simulation to match the solar adiabat, it is encouraging that the change in K is relatively modest. Comparisons such as the one attempted here are undoubtedly important tests of simulations of solar convection.

2.4. HOW ADIABATIC IS THE DEEP PART OF THE CONVECTION ZONE?

The approximation used in equation (1) is only valid if γ is constant. However, to the extent that the stratification can be assumed to be adiabatic, p and ρ are related by

$$\frac{d \ln p}{d \ln \rho} = \gamma_1 \equiv \left(\frac{\partial \ln p}{\partial \ln \rho} \right)_s, \quad (17)$$

where the dependence of γ_1 on p , ρ and composition is determined by the equation of state of the gas. It follows that the structure of the adiabatic part of the convection zone is entirely specified by the equation of state, the composition and the actual value s_{ad} of the specific entropy. This property makes the adiabatic part of the convection zone a valuable tool for investigations of the equation of state of stellar material (*e.g.* Christensen-Dalsgaard & Däppen 1992) and forms the basis for helioseismic determinations of the solar envelope helium abundance (*e.g.* Kosovichev *et al.* 1992).

It is evident that these analyses are possible only to within the accuracy of equation (17). Since the thermodynamic effects under consideration are minute, this imposes severe constraints on the superadiabatic gradient. The behaviour for three different treatments of convection, in relation to the location of the dominant ionization zones, was illustrated in Fig. 1. In the hydrogen and, at least for MLT, the first helium ionization zone $\nabla - \nabla_{\text{ad}} \sim 10^{-3}$, which is comparable with the effects introduced by current uncertainties in the equation of state. Thus investigations of the equation of state have generally been concentrated on the second helium ionization zone, where $\nabla - \nabla_{\text{ad}}$ is at most around 10^{-4} in the MLT model. According to the CM formulation, where convective efficiency increases rapidly with depth, the allowable range might include also the first helium ionization zone. The hydrodynamical simulations do not extend sufficiently deeply to reach the second helium ionization zone but appear, from Fig. 1, to yield a superadiabatic gradient intermediate between MLT and CM. These substantial differences indicate that the uncertainty in the treatment of convection might have a significant influence on the degree of adiabaticity even in the second helium ionization zone. These issues need further investigation, before very detailed tests of the equation of state and/or precise determination of the helium abundance can be carried out.

I finally note that turbulent pressure might also influence tests of the thermodynamic properties of the solar plasma. For example, the ratio between the turbulent and total pressure at the upper edge of the second helium ionization zone in the MLT Model 2 can be estimated as approximately 10^{-4} . This could have significant effects on the relation between γ_1 , p , ρ and composition inferred from helioseismic analyses.

3. Helioseismic data on solar models

Extensive reviews on solar oscillations and their application to helioseismology were given, *e.g.*, by Gough & Toomre (1991), Christensen-Dalsgaard & Berthomieu (1991), Gough & Thompson (1991) and Gough (1993). Since I consider only the spherically symmetric structure, the oscillation frequencies ω_{nl} depend on the degree l and radial order n alone. I shall assume the adiabatic approximation, neglecting the energy gain or loss of the oscillations. This is an excellent approximation in almost the entire Sun but breaks down in the near-surface region where the thermal time scale becomes comparable with the oscillation period. As discussed in detail by Rosenthal (these proceedings) this region gives rise to other uncertainties in the computation of the frequencies, arising from the physics of the model and the oscillations; thus in any case the presence of errors in the computed frequencies, arising from the near-surface region, must be kept in mind.

The observed frequencies correspond mostly to acoustic modes. These are trapped between an upper turning point just below the photosphere and a lower turning point, at a distance r_t from the centre determined by

$$\frac{c(r_t)}{r_t} = \frac{\omega}{l + 1/2}, \quad (18)$$

where c is the adiabatic sound speed. It follows from equation (18) that high-degree modes are trapped near the solar surface whereas low-degree modes penetrate into the solar core.

Perturbation analysis of the oscillation equations (*e.g.* Christensen-Dalsgaard & Berthomieu 1991; see also Rosenthal, these proceedings) shows that the near-surface effects cause changes in the frequencies of the form

$$\delta\omega_{nl}^{(\text{ns})} = \frac{F_{\text{surf}}(\omega_{nl})}{Q_{nl}}, \quad (19)$$

for modes of low or moderate degree. Here $Q_{nl} = E_{nl}/\bar{E}_0(\omega_{nl})$, where E_{nl} is the mode energy, normalized by the squared surface amplitude, and $\bar{E}_0(\omega_{nl})$ is the energy of a radial ($l = 0$) mode, interpolated to ω_{nl} . Thus the behaviour of Q_{nl} reflects the variation of the turning-point radius r_t with the degree of the mode: high-degree modes involve a smaller part of the Sun

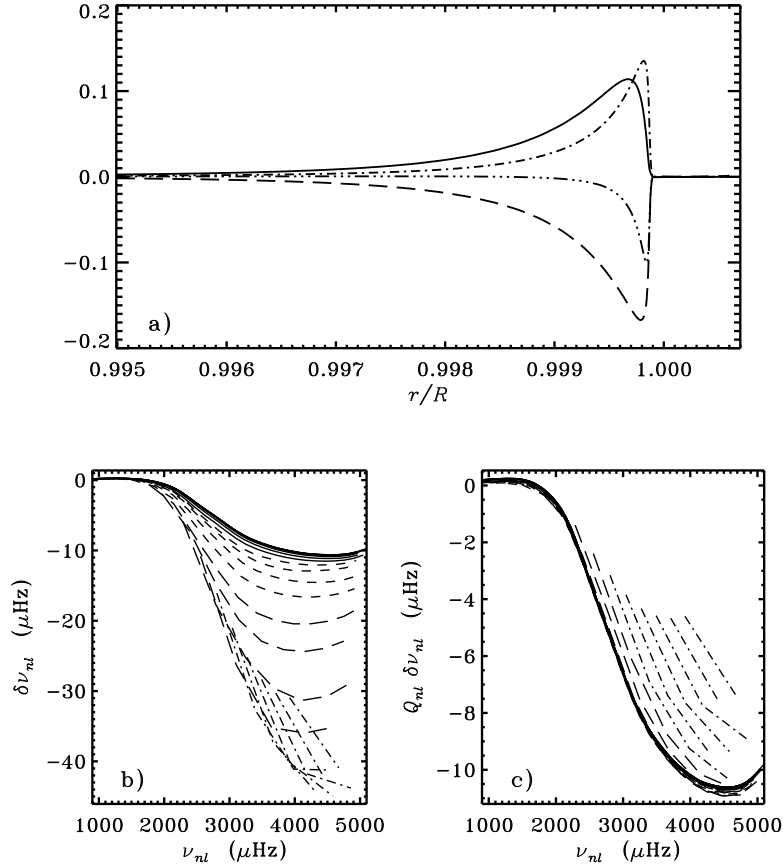


Figure 3. (a) Differences, at fixed mass, between Model 1 and Model 2 of Table 1, computed with the CM and the MLT convection formulations, in the sense (CM) – (MLT). The following differences are shown: $\delta \ln c^2$ (solid line); $\delta \ln \rho$ (dashed line); $\delta \ln T$ (dot-dashed line); and $\delta \ln \gamma_1$ (triple-dot-dashed line). (b) Unscaled frequency differences between the same two models, for the following degrees: $l = 0 - 30$ (solid lines); $l = 40, 50, 70, 100$ (short dashed lines); $l = 150, 200, 300, 400$ (long dashed lines); and $l = 500, 600, 700, 800, 900, 1000$ (dot-dashed lines). (c) Corresponding scaled frequency differences, using the same line styles.

than do low-degree modes and therefore have smaller normalized energy and Q_{nl} , hence according to equation (19) making their frequencies more susceptible to the near-surface effects. $F_{\text{surf}}(\omega)$ is a function of frequency which depends on the physics of the near-surface region; it may be shown that if the errors in the calculation are confined extremely close to the surface, F_{surf} is a slowly varying function of ω which is small at low frequency.

Equation (19) motivates analyzing frequency differences in terms of

$Q_{nl}\delta\omega_{nl}$. This scaling effectively reduces the frequency change resulting from near-surface effects to the equivalent change for a radial mode, by taking out the dependence on the penetration depth. Thus if differences in structure were confined exclusively to the near-surface region, we might expect $Q_{nl}\delta\omega_{nl}$ to depend on frequency alone, for modes of low or moderate l for which the motion in the surface layers is almost radial.

These principles may be illustrated by comparing Models 1 and 2 computed with the CM and MLT treatments of convection and, according to Fig. 2, differing only very near the surface. Figure 3a shows differences, at fixed mass, between these models; as discussed by Christensen-Dalsgaard & Thompson (1996) the effects of near-surface model changes are most naturally represented in terms of such differences. It is evident that the change in the model is essentially confined to the superadiabatic region where the temperature gradients differ substantially. Unscaled and scaled frequency differences between these two models are shown in panels (b) and (c) of Fig. 3. The unscaled differences show a fairly substantial dependence on degree which is largely suppressed by the scaling, except at high degree.

It is convenient to relate frequency differences between two models, or between the Sun and a model, to the corresponding differences in structure. This is generally done on the assumption that the differences are sufficiently small that the relation is linear. Asymptotic theory for acoustic modes then shows that (Christensen-Dalsgaard, Gough & Pérez Hernández 1988)

$$S_{nl} \frac{\delta\omega_{nl}}{\omega_{nl}} = \mathcal{H}_1 \left(\frac{\omega_{nl}}{l + 1/2} \right) + \mathcal{H}_2(\omega_{nl}), \quad (20)$$

where S_{nl} is closely related to the scaling Q_{nl} introduced in equation (19),

$$\mathcal{H}_1(w) = \int_{r_t}^R \left(1 - \frac{c^2}{r^2 w^2} \right)^{-1/2} \frac{\delta_r c}{c} \frac{dr}{c}, \quad (21)$$

and the function $\mathcal{H}_2(\omega)$ contains contributions from the near-surface region, including the uncertain aspects of the physics. In equation (21) the difference $\delta_r c$ is evaluated at fixed radius r .

Figure 4a shows differences between the first year's observations with the LOWL instrument (Tomczyk *et al.* 1995; Tomczyk, Schou & Thompson 1996) and Model S of Christensen-Dalsgaard *et al.* (1996), scaled as suggested by equation (19). Clearly the frequency differences depend primarily on frequency. This suggests that the differences between the Sun and the model are dominated by the near-surface effects. Indeed, the shape and magnitude of the differences are rather similar to the differences, shown in Fig. 3, between the CM and MLT models. This might suggest that the CM formulation may be a more accurate representation of the uppermost layers

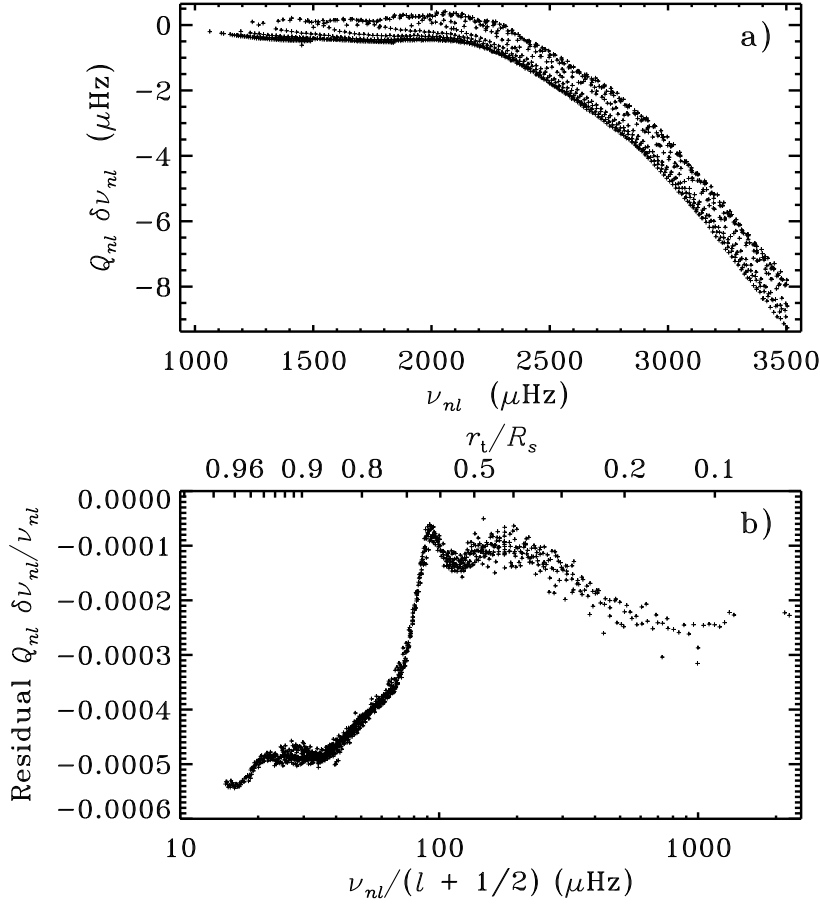


Figure 4. (a) Scaled differences between cyclic frequencies $\nu = \omega/2\pi$ observed with the LOWL instrument (Tomczyk *et al.* 1995) and frequencies of Model S of Christensen-Dalgaard *et al.* (1996), in the sense (Sun) – (Model). Modes of degree $l = 0 - 99$ are included. (b) Residual scaled relative frequency differences, after subtraction of the function $\mathcal{H}_2(\omega)$ obtained from a fit of the form (20). The upper abscissa shows the turning-point radius r_t , related to $\omega/(l + 1/2)$ through equation (18).

of the solar convection zone (*e.g.* Paternò *et al.* 1993); however, as discussed by Rosenthal (these proceedings) this conclusion may be premature, given the other potential near-surface contributions to the frequency differences.

Equation (20) indicates that the relative frequency differences can be separated into a contribution depending on frequency and a contribution depending on $\omega/(l + 1/2)$ or, equivalently, the turning-point radius r_t . Indeed, by fitting this relation to relative differences corresponding to those shown in Fig. 4a and subtracting the component corresponding to $\mathcal{H}_2(\omega)$

one obtains the residuals shown in Fig. 4b which are clearly predominantly a function of $\omega/(l + 1/2)$. The most striking feature is the rapid variation for modes whose turning points are near $0.7R$, *i.e.*, close to the base of the convection zone. According to equation (21) this suggests that there is a comparatively large component of the sound-speed difference at this point; as we shall see in the next section, this is in fact the case.

4. Structure of the radiative interior

To investigate the causes of the residual frequency differences shown in Fig. 4b a more careful analysis is required. In particular, it is preferable to move beyond the asymptotic approximation in equation (20). From general properties of the oscillation equations one may express small differences in adiabatic frequency linearly in terms of differences in two variables characterizing the model, *e.g.* $\delta_r c^2$ and $\delta_r \rho$ (*e.g.* Gough & Thompson 1991). The actual differences between the observed frequencies and adiabatic frequencies of a model must also reflect the nonadiabatic effects on the frequencies and the inadequacies in the modelling of the near-surface region. As a result, the frequency differences can be expressed as

$$\frac{\delta\omega_{nl}}{\omega_{nl}} = \int_0^R \left[K_{c^2,\rho}^{nl}(r) \frac{\delta_r c^2}{c^2}(r) + K_{\rho,c^2}^{nl}(r) \frac{\delta_r \rho}{\rho}(r) \right] dr + Q_{nl}^{-1} \mathcal{G}(\omega_{nl}) + \epsilon_{nl}, \quad (22)$$

ϵ_{nl} being the observational error; here the kernels $K_{c^2,\rho}^{nl}$ and K_{ρ,c^2}^{nl} are determined from the eigenfunctions in the model, while the penultimate term arises from the neglected physics in the near-surface region.

Equation (22) forms the basis for inverse analyses to infer properties of $\delta_r c$ and $\delta_r \rho$. Here I consider the so-called subtractive optimally localized averages (SOLA) technique, first introduced by Pijpers & Thompson (1992); details of the implementation were provided by Basu *et al.* (1996a). The principle is to construct linear combinations of equation (22) with weights $c_{nl}(r_0)$ chosen such that the *averaging kernel*

$$\mathcal{K}_{c^2,\rho}(r_0, r) = \sum_{nl} c_{nl}(r_0) K_{c^2,\rho}^{nl}(r) \quad (23)$$

is a function localized near $r \simeq r_0$, whereas the remaining terms on the right-hand side of equation (22) are minimized. In particular, the contribution from the near-surface problems, as given by the term in $\mathcal{G}(\omega)$, can largely be eliminated. To the extent that this procedure is successful, we obtain a localized estimate of $(\delta_r c/c)(r_0)$,

$$\overline{\left(\frac{\delta_r c}{c} \right)}(r_0) = \sum_{nl} c_{nl}(r_0) \frac{\delta\omega_{nl}}{\omega_{nl}} \simeq \int_0^R \mathcal{K}_{c^2,\rho}(r_0, r) \frac{\delta_r c^2}{c^2}(r) dr. \quad (24)$$

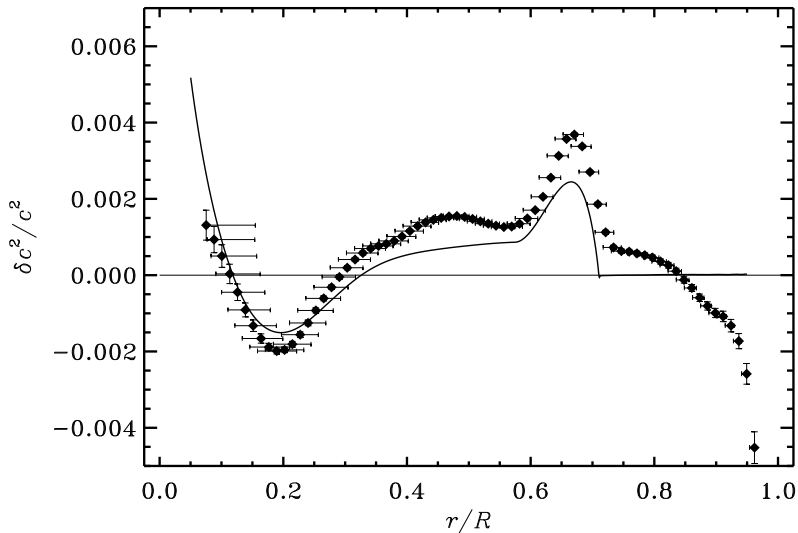


Figure 5. The symbols show results of SOLA inversion (Basu *et al.* 1996b) of frequencies obtained with the the LOWL instrument (Tomczyk *et al.* 1995), to infer the sound-speed difference between the Sun and Model S of Christensen-Dalsgaard *et al.* (1996), in the sense (Sun) – (Model). The vertical error bars show the standard error in the result, obtained from the estimated errors in the observed frequencies, whereas the horizontal bars indicate the extent of the averaging kernels (*cf.* equation 23). The curve shows the change in squared sound speed resulting from the modification to the hydrogen profile illustrated in Fig. 6 (*cf.* Bruntt 1996).

An estimate of the standard error in the result can be obtained from the observational standard deviations of ϵ_{nl} .

Figure 5 shows the difference in squared sound speed resulting from an application of this procedure to the frequency differences illustrated in Fig. 4a (Basu *et al.* 1996b). It is evident that there is indeed a sharp feature in the sound-speed difference just below the convection zone; this is responsible for the behaviour of the residual frequency differences around $\nu/(l+1/2) \simeq 80 \mu\text{Hz}$ in Fig. 4b. A second substantial feature is the dip in $\delta_r c^2/c^2$ around $r \simeq 0.2R$, *i.e.*, at the edge of the nuclear-burning core, apparently followed by a rise in the deeper parts of the core. In the convection zone the difference is relatively small, although with a rise in magnitude towards the surface; this might be caused by errors in the equation of state or possibly by residual effects of the near-surface problems.

To discuss the possible causes for the sound-speed differences in the radiative interior I note that, according to the ideal gas law,

$$c^2 = \frac{\gamma_1 p}{\rho} \simeq \frac{\gamma_1 k_B T}{\mu m_u}, \quad (25)$$

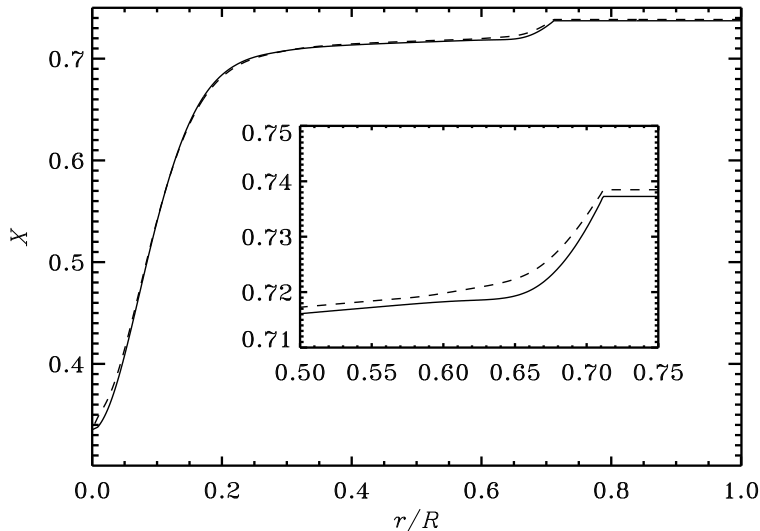


Figure 6. Profiles of the abundance X by mass of hydrogen. The solid line shows the profile in Model S of Christensen-Dalsgaard *et al.* (1996), whereas the dashed line shows a modified profile aimed at trying to match the sound-speed difference shown in Fig. 5 between the Sun and the model. The insert provides a blow-up of the region around the base of the convection zone. Adapted from Bruntt (1996).

where k_B is Boltzmann's constant, μ is the mean molecular weight and m_u is the atomic mass unit. Thus $\delta_r c/c$ must reflect a difference in T/μ between the Sun and the model. With this in mind, it is striking that the two regions of dramatic variation in $\delta_r c/c$ coincide with regions where the composition, and hence μ , varies strongly. This is illustrated by the hydrogen profile shown in Fig. 6: beneath the convection zone the accumulation of helium settling out of the convection zone causes a sharp gradient in X , whereas hydrogen burning, with an additional small contribution from helium settling, leads to a strong variation of X in the core. In both cases, the difference between the solar and model sound speed could be reduced by smoothing the composition profile: this would increase X , reduce μ and hence increase c just below the convection zone and similarly reduce X and c at the edge of the core, with a corresponding increase in the inner core.

To test this possibility, Bruntt (1996) adjusted the hydrogen profile in Model S in such a way as to approximate the sound-speed difference shown in Fig. 5. The profiles were constrained to correspond to the same total amount of hydrogen as for Model S, to within 0.5 %, and to give the observed solar luminosity; however, no assumptions were made about possible physical mechanisms which might cause the redistribution of hydrogen. The

resulting profile is shown in Fig. 6 as a dashed line, and the difference in sound speed between the modified model and Model S was shown as the solid line in Fig. 5. Evidently the change in composition has reproduced much of the sound-speed difference between the Sun and the model. Evidence for a smoother composition profile just below the convection zone was also found from inverse analysis by Antia & Chitre (1996).

Such changes in composition are not implausible. Indeed, as mentioned in the introduction, the depletion of lithium and beryllium demonstrates that mixing in the Sun well below the convection zone must have taken place at some stage during solar main-sequence evolution. Computations with rotationally-induced mixing accounting for the lithium depletion (Chaboyer *et al.* 1995; Richard *et al.* 1996; see also Zahn, these proceedings) have largely succeeded in eliminating the bump in the sound-speed difference just below the convection zone (Gough *et al.* 1996). Mixing would also be caused by convective penetration into the stable region; even a very small fraction of convective eddies penetrating to a substantial distance could cause appreciable mixing, with little effect on the temperature structure. It has furthermore been suggested that gravity waves excited by convective penetration might lead to mixing (*e.g.* Montalbán 1994; Montalbán & Schatzman 1996; see also Schatzman, these proceedings).

It should be noted that the lithium depletion and change in the hydrogen profile are not automatically related: thus strong mixing in the early phases of solar evolution, as might have been caused by rotation, could have depleted lithium with little effect on the present hydrogen profile. In this sense, the information obtained from lithium and from the sound-speed inversion is complementary.

Unfortunately, mixing is not the only mechanism that might account for the sound-speed results. Early mass loss (*e.g.* Guzik & Cox 1995) might also reduce the lithium and beryllium abundances, and in addition improve the agreement with the inferred solar sound speed just below the convection zone (Gough *et al.* 1996). Furthermore, it is obviously possible to change the sound speed by changing the temperature profile. This requires modifications to the opacity such that the condition of radiative energy transport is satisfied. Tripathy, Basu & Christensen-Dalsgaard (1996) showed that the inferred sound-speed difference in Fig. 5 can be reproduced by means of a suitably chosen opacity modification of only a few per cent. Thus independent information and, if possible, tighter constraints on the opacity are required to separate the different possible causes for the remaining differences between the Sun and solar models.

5. Discussion

The results of inversion for the sound-speed difference, such as those shown in Fig. 5, indicate a strikingly close agreement between the solar sound speed and that of normal solar models. This has little implication for the dynamics of the upper parts of the convection zone which have been adjusted, by calibration of the mixing length, to produce a model with the correct radius; however, it does indicate that conditions at and below the base of the convection zone are not vastly different from those obtained from normal stellar modelling (see also Roxburgh, these proceedings). Nonetheless, the most dramatic sound-speed difference does in fact occur in this region. Although various explanations are possible, the most plausible of these is perhaps mixing induced by rotational instability, direct convective penetration or gravity waves. However, it is important to stress that, despite its great power, helioseismology cannot on its own provide a full investigation of the problems of mixing in stellar interiors. This requires a combination of a better physical understanding of the mixing processes, data from other stars on, for example, the lithium depletion (*e.g.* Michaud & Charbonneau 1991), and tighter constraints on other aspects of the physics of the radiative interior, such as the opacity.

It is encouraging that the hydrodynamical simulations discussed here result in a structure of the adiabatic part of the convection zone fairly close to that obtained in calibrated parametrized models. This offers some hope that such simulations might be used to provide a firmer extrapolation to other stars than the commonly used assumption of a constant mixing-length parameter (Ludwig, Freytag & Steffen, these proceedings; Trampedach *et al.*, these proceedings). Tests of such extrapolations might be provided by well-observed binary stars, such as the α Cen system (*e.g.* Edmonds *et al.* 1992; Fernandes & Neuforge 1995). Observations of solarlike oscillations in these or other stars might clearly be extremely valuable in constraining the models, in terms of the properties of convection or other aspects of the structure. When such data are available, the meaning of the “S” in the title of subsequent conferences in this series might be subtly changed.

Acknowledgements

I am grateful to Hans Bruntt for permission to show the results of the modified hydrogen profile in Figs 5 and 6, to Regner Trampedach for the matched envelope and hydrodynamical simulation and to Mario Monteiro for the implementation of the CM formalism. Colin Rosenthal is thanked for comments on an earlier version of the paper. This work was supported by the Danish National Research Foundation through its establishment of the Theoretical Astrophysics Center.

References

- Anders E. & Grevesse N., 1989. *Geochim. Cosmochim. Acta* **53**, 197
- Antia H. M. & Chitre S. M., 1996. Submitted to *ApJ*.
- Böhm-Vitense E., 1958. *Z. Astrophys.* **46**, 108
- Basu S., Christensen-Dalsgaard J., Pérez Hernández F. & Thompson M. J., 1996a. *MNRAS* **280**, 651
- Basu S., Christensen-Dalsgaard J., Schou J., Thompson M. J. & Tomczyk S., 1996b. *Bull. Astron. Soc. India* **24**, 147
- Bruntt H., 1996. *Batchelor thesis*, Aarhus University.
- Canuto V. M. & Mazzitelli I., 1991. *ApJ* **370**, 295
- Chaboyer B., Demarque P., Guenther D. B. & Pinsonneault M. H., 1995. *ApJ* **446**, 435
- Christensen-Dalsgaard J. & Däppen W., 1992. *A&AR* **4**, 267.
- Christensen-Dalsgaard J. & Berthomieu G., 1991. In *Solar interior and atmosphere*, eds Cox A. N., Livingston W. C. & Matthews M., Space Science Series, University of Arizona Press, p. 401
- Christensen-Dalsgaard J. & Thompson M. J., 1991. *ApJ* **367**, 666
- Christensen-Dalsgaard J. & Thompson M. J., 1996. *MNRAS*, in the press.
- Christensen-Dalsgaard J., Däppen W., Ajukov S. V. *et al.*, 1996. *Science* **272**, 1286
- Christensen-Dalsgaard J., Gough D. O. & Pérez Hernández F., 1988. *MNRAS* **235**, 875
- Christensen-Dalsgaard J., Gough D. O. & Thompson M. J., 1991. *ApJ* **378**, 413
- Edmonds P., Cram L., Demarque P., Guenther D. B. & Pinsonneault M. H., 1992. *ApJ* **394**, 313
- Fernandes J. & Neuforge C., 1995. *A&A* **295**, 678
- Gough D. O., 1993. In *Astrophysical fluid dynamics, Les Houches Session XLVII*, eds Zahn J.-P. & Zinn-Justin J., Elsevier, Amsterdam, 399
- Gough D. O. & Thompson M. J., 1991. In *Solar interior and atmosphere*, eds Cox A. N., Livingston W. C. & Matthews M., Space Science Series, University of Arizona Press, p. 519
- Gough D. O. & Toomre J., 1991. *ARA&A* **29**, 627
- Gough D. O. & Weiss N. O., 1976. *MNRAS* **176**, 589
- Gough D. O., Kosovichev A. G., Toomre J. *et al.*, 1996. *Science* **272**, 1296
- Guzik J. A. & Cox A. N., 1995. *ApJ* **448**, 905
- Iglesias C. A., Rogers F. J. & Wilson B. G., 1992. *ApJ* **397**, 717
- Kosovichev A. G. & Fedorova A. V., 1991. *Astron. Zh.* **68**, 1015 (English translation: *Sov. Astron.* **35**, 507)
- Kosovichev A. G., *et al.*, 1992. *MNRAS* **259**, 536
- Michaud G. & Charbonneau P., 1991. *Space Sci. Rev.* **57**, 1
- Michaud G. & Proffitt C. R., 1993. In *Proc. IAU Colloq. 137: Inside the stars*, eds Baglin A. & Weiss W. W., *ASP Conf. Ser.* **40**, 246
- Montalbán J., 1994. *A&A* **281**, 421
- Montalbán J. & Schatzman E., 1996. *A&A* **305**, 513
- Paternò L., Ventura R., Canuto V. M. & Mazzitelli I., 1993. *ApJ* **402**, 733
- Pijpers F. P. & Thompson M. J., 1992. *A&A* **262**, L33
- Richard O., Vauclair S., Charbonnel C. & Dziembowski W. A., 1996. *A&A* **312**, 1000
- Rogers F. J., Swenson F. J. & Iglesias C. A., 1996. *ApJ* **456**, 902
- Schwarzschild M., 1958. *Structure and evolution of the stars*, Princeton University Press, Princeton, New Jersey.
- Stein R. F. & Nordlund Å., 1989. *ApJ* **342**, L95
- Tomczyk S., Schou J. & Thompson M. J., 1996. *Bull. Astron. Soc. India* **24**, 245
- Tomczyk S., *et al.*, 1995. *Solar Phys.* **159**, 1
- Tripathy S. C., Basu S. & Christensen-Dalsgaard J., 1996. In *Sounding Solar and Stellar Interiors. Proc. IAU Symposium No 181, poster volume*, eds Provost J. & Schieder F. X., in the press.